Osteoprotegerin: a double-edged sword in osteoarthritis development

Rodriguez Ruiz, A.

CHAPTER 4

Mutation in the CCAL1 locus accounts for bidirectional process of human subchondral bone turnover and cartilage mineralization

Alejandro Rodríguez Ruiz[1§], Marcella van Hoolwerff[1§], Sara Sprangers[2], Eka Suchiman[1], Ton Schoenmaker[2,3], Petra Dibbets-Schneider[4], Johan L. Bloem[4], Rob GHH Nelissen[7], Christian Freund[5,6], Christine Mummery[5,6], Vincent Everts[2], Teun J. de Vries[3], Yolande FM Ramos[1*#], and Ingrid Meulenbelt[1*]

[1]Dept. Biomedical Data Sciences, Section Molecular Epidemiology, Leiden University Medical Center, Leiden (LUMC), The Netherlands; [2]Dept. Oral Cell Biology, [3]Dept. Periodontology, Academic Centre for Dentistry Amsterdam (ACTA), University of Amsterdam (UvA) and Vrije University (VU) Amsterdam, 1081 LA Amsterdam, The Netherlands; [4]Dept. Radiology, LUMC; [5]Dept. Anatomy, LUMC; [6]LUMC iPSC Core Facility. [7]Dept. Orthopedics LUMC, Leiden, The Netherlands.

[§]Contributed equally.
[*]Shared last.

Rheumatology (Oxford). 2022;00:1-13

ABSTRACT:

Objectives: To study the mechanism by which the readthrough mutation in *TNFRSF11B*, encoding osteoprotegerin (OPG) with additional 19 amino acids at its C-terminus (OPG-XL), causes the characteristic bidirectional phenotype of subchondral bone turnover accompanied by cartilage mineralization in chondrocalcinosis patients.

Methods: OPG-XL was studied by human induced pluripotent stem cells expressing OPG-XL and two isogenic CRISPR/Cas9-corrected controls in cartilage and bone organoids. Osteoclastogenesis was studied with monocytes from OPG-XL carriers and matched healthy controls followed by gene expression characterization. DEXA scans, and MRI analyses were used to characterize the phenotype of carriers and non-carriers of the mutation.

Results: Human OPG-XL carriers relative to sex- and age-matched controls showed, after an initial delay, large active osteoclasts with high number of nuclei. By employing hiPSCs expressing OPG-XL and isogenic CRISPR/Cas9-corrected controls to established cartilage and bone organoids, we demonstrated that expression of OPG-XL resulted in excessive fibrosis in cartilage and high mineralization in bone accompanied by marked downregulation of *MGP* and upregulation of *DIO2* gene expression, respectively.

Conclusions: The readthrough mutation at CCAL1 locus in *TNFRSF11B* identifies an unknown role for OPG-XL in subchondral bone turnover and cartilage mineralization in humans via DIO2 and MGP functions. Previously, OPG-XL was shown to affect binding between RANKL and heparan sulphate (HS) resulting in loss of immobilized OPGXL. Therefore, effects may be triggered by deficiency in the immobilization of OPG-XL Since the characteristic bidirectional pathophysiology of articular cartilage calcification accompanied by low subchondral bone mineralization is also a hallmark of OA pathophysiology, our results are likely extrapolated to common arthropathies.

Key messages:

- OPG-XL mutation directly affects chondrocyte and osteoblast states towards matrix mineralization mediated by respectively MGP and DIO2.
- Expression of OPG-XL drives accumulation of large active osteoclasts with high number of nuclei.
- Interference with OPG–RANKL–heparan sulphate underlying concurrent cartilage calcification and subchondral bone loss likely extrapolates to common arthropathies.

INTRODUCTION

Joint tissue degeneration during osteoarthritis (OA) is a complex multistep process characterized by pathogenic bidirectional process of subchondral bone turnover and cartilage mineralization (1, 2). It has been suggested that this characteristic inverse mineralization process has shared mechanisms with the frequently observed concurrent pathogenic bone turnover and vasculature mineralization (2, 3). Key proteins likely involved are osteoprotegerin (OPG), a decoy receptor of osteoclastogenesis (4) and matrix Gla protein (MGP), a vitamin K dependent inhibitor of ectopic bone formation (5) since overexpression or knockdown of these genes in murine models results in such inverse pathological mineralization process (6-8). The inverse causal role of dysfunctional OPG in human joint tissue mineralization was demonstrated by identification of a readthrough mutation (c1205A=T; p.Stop402Leu) in *TNFRSF11B* encoding OPG at the chondrocalcinosis locus 1 (CCAL1) (9) in multiple families worldwide (10-12). In these families CCAL1 phenotype is defined by early onset OA with different levels of articular cartilage calcification i.e. chondrocalcinosis (13) and low subchondral bone mineralization (12).

OPG is a well-known soluble decoy receptor competing with receptor activator of nuclear factor (RANK) expressed at osteoclasts for binding to nuclear factor kB ligand (RANKL) (14). Binding of RANKL to RANK is driving osteoclastogenesis hence bone turnover, while binding to OPG inhibits this process (15). Pleiotropic functions of OPG and RANKL were more recently suggested by showing that RANKL stimulates osteoclast fission to produce transcriptionally distinct osteomorphs which in turn recycle towards large multinucleated osteoclasts or polykaryons by fusion under tight control of OPG (15). Although binding of OPG to RANKL, established by N-terminal domains of OPG, is frequently studied, less is known about the interaction of OPG via its C-terminus with membrane bound heparan sulphate (HS) on osteoblasts (16). A binding that appears indispensable for RANKL mediated inhibition of osteoclastogenesis due to immobilization of secreted OPG on the osteoblast membrane and formation of a stable HS-OPG-RANKL complex (16, 17). In line with this, the CCAL1 readthrough mutation, adding an additional 19 amino acids to the C-terminus of OPG, denoted OPG-XL, has been shown to hamper OPG-HS binding hence permitting osteoclastogenesis and bone turnover (11). This explains characteristic low subchondral bone density in affected CCAL1 family members (12) and sporadic cases (18).

The mechanism by which OPG-XL results in cartilage calcification remains, however, elusive. In fact, a robust role of *TNFRSF11B* and its ligand *TNFSF11* encoding RANKL particularly in cartilage (patho)physiology has been highlighted by transcriptome wide studies. Herein, *TNFRSF11B* and *TNFSF11* but not *TNFRSF11A* encoding RANK show high expression and are robustly responsive to OA cartilage pathophysiology as marked by consistent high upregulation in

human OA affected relative to preserved (19-21) or healthy (22) cartilage. In contrast, differential expression of *TNFRSF11B* or *TNSF11* in subchondral bone underlying preserved and lesioned areas of OA cartilage was not observed (23). Other than that, with *TNFSF11* being a robust OA risk gene identified in the largest genome-wide association study to date (24), aberrant function of OPG/RANKL also underlies common OA aetiopathology.

Here, we set out to functionally characterize the effects of OPG-XL in joint tissues by employing mutated and control human primary chondrocytes, as well as human induced pluripotent stem cells (hiPSCs) from affected CCAL1 family members and CRISPR/Cas9 repaired hiPSCs isogenic controls, to established *in vitro* organoid models of cartilage and bone (25). Additionally, to study the effect of OPG-XL in human osteoclastogenesis, monocytes isolated from blood of carriers of the mutation were compared to monocytes of age- and sex-matched controls in osteoclastogenesis assays. Altogether, we aimed to decipher effects of OPG-XL on joint tissue mineralization that could explain the CCAL1 phenotype of articular cartilage calcification in concurrence with low subchondral bone mineralization. Given that subchondral bone turnover and cartilage calcification are general hallmarks of OA pathophysiology and at the molecular level involve *TNFRSF11B* and *TNFSF11,* our results are likely of relevance to common OA.

MATERIALS AND METHODS

Study participants

Within the Familial early-onset Osteoarthritis (FOA) study, 13 family members were incorporated (six females and seven males aged 23-62 years with mean age 47 years; **Supplementary Table S1**). Cartilage samples were collected within the ongoing Research Arthritis and Articular Cartilage (RAAK) study from five common OA patients and one family member undergoing total joint replacement surgery (RAAK: two females and three males aged 50–87 years with mean age 73 years; FOA: female aged 61).

Genotyping and radiographic analyses

FOA family members were genotyped with in-house genetic test developed by Department of Clinical Genetics to determine presence or absence of previously identified readthrough mutation in *TNFRSF11B* (OPG-XL; **Figure 1A**), (9) and were characterized by dual energy X-ray absorptiometry (DEXA) as well as radiographs and magnetic resonance imaging (MRI) of the knees to respectively determine BMD and OA severity, (dual energy X-ray absorptiometry) as well as radiographs and MRI (magnetic resonance imaging) of the knees to respectively determine bone mineral density (BMD) and OA severity (**Supplementary Table S2** and

S3; **Figure 1B**). DEXA scans of 253 controls were used to compare results to the general population. OA features were scored based on semi quantitative MRI OA knee score (MOAKS(1)) highlighting different characteristics (e.g. bone marrow lesions, osteophytes, cysts, and loss of cartilage full thickness) at 14 articular subregions in the knee.

Generation, characterization and CRISPR/Cas9 correction of OPG-XL patient hiPSCs

Human iPSCs were generated by the LUMC iPSC core facility as described before (26) from skin fibroblasts of a FOA participant, carrier of the mutation resulting in expression of OPG-XL (line LUMC0103iOPG). Pluripotency and spontaneous differentiation were assessed, and cells were karyotyped after 15 passages (**Supplementary Figure S1A-C**). Cells were maintained under standard conditions (37°C, 5% CO_2) in TeSR-E8 medium (STEMCELL Technologies).

To obtain two independent isogenic hiPSC controls without the mutation (lines B89 and C81), CRISPR/Cas9 correction of the mutation was performed for the OPG-XL hiPSCs (LUMC0103iOPG). sgRNAs were designed by *in silico* tools (Rgenome.net and MultiCrispr.net) and selected based on predicted highest specificity and least off-target effects: gRNA1 (5'-AAAAATAAGCTGCTTATTACTGG-3'), and gRNA2 (5'-AAGCTGCTTATTA CTGGAAATGG-3'). The sgRNAs were cloned into a CRISPR/Cas9 plasmid carrying sequences for expression of green fluorescent protein (PX458), and co-transfected using Lipofectamine Stem Reagent (Thermo Fisher Scientific Inc) with a single-stranded oligo donor repair template (ssODN 5'-CACTGAAAGCCTCAAGTGCCTGAGAAACAGTTTACTCATCCATGGGATCTCGC-CAATTGTGAGGAAACAGCTCAATGGCGATTTCGAGTTATAAGCAGCTTATTTTTACT-GATTGGACCTGGTTACC-3') to achieve homologous directed repair (HDR). Twenty-four hours after transfection of gRNAs and ssODN, single-cell-sorting for green fluorescent protein positive cells was performed with FACSAria-I (BD Biosciences), and hiPSCs were seeded at low density (270 cells/cm^2) for clonal expansion. After eight days, colonies were collected and reseeded as single-cells in 96-well plates with TESR-E8 and CloneR (STEMCELL Technologies). DNA was obtained from single colonies using Quick Extract (Lucigen). Region of interest was amplified with PCR and screening for homozygous CRISPR/Cas9-corrected colonies (wt) was done by restriction with PsiI (New England Biolabs). Two homozygous clones (B89 and C81 from gRNA2 and gRNA1, respectively) were identified and repair of the readthrough mutation was confirmed by Sanger sequencing (**Supplementary Figure S1D-F**).

Human primary chondrocytes

Human primary chondrocytes were collected from OA patients (RAAK study; N=5 donors) and carrier of OPG-XL (FOA study; N=1 donor) undergoing joint replacement surgery. Collection, expansion, and deposition of cartilage extracellular matrix of primary chondrocytes has been previously described (20).

Chondrogenesis and osteogenesis of iPSCs

Mesenchymal stromal cells were generated from hiPSC (hiMSCs) of the OPG-XL hiPSCs (LUMC0103iOPG) and of the two thereof derived CRISPR/Cas9 isogenic control hiPSCs (B89 and C81) using Stemcell Technologies' Mesenchymal Progenitor Kit following the manufacturer's instructions. Chondrogenesis and osteogenesis was performed in organoids following our established protocol employing 750000 cells per organoid as described before (25). Cells were counted with the Nucleocounter NC-200 (Chemometec).

Isolation of blood cells and osteoclastogenesis

Peripheral blood mononuclear cells (PBMCs) were isolated from whole blood of six FOA members with mutation and six sex- and age- matched controls (characteristics of donors in **Supplementary Table S4**) using Ficoll density gradient centrifugation as previously described (27). CD14-positive monocytes were collected by negative selection using magnetic MACS microbeads according to the manufacturer's instructions. Cells were then seeded onto slices of human tibia bone of healthy individuals and cultured in medium composed of α-MEM supplemented with 10% fetal calf serum (HyClone I, Thermo Fisher Scientific Inc) and antibiotics following pre-treatment with 10 ng/ml macrophage colony-stimulating factor (M-CSF, R&D Systems) for three days. Osteoclastogenesis was induced by addition of 2 ng/ml RANKL (R&D Systems) in the presence of 10 ng/ml M-CSF. Cultures were maintained at 37°C and 5% CO2 with medium refreshed twice weekly.

CTX-1 measurement and resorption-pit assay

Concentration of C-terminal telopeptide of type 1 collagen (CTX-1) in conditioned media following 14 or 21 days culture on slices of human tibia bone was determined with ELISA (Immunodiagnostic System, Inc) according to the manufacturer's protocol. Measurements were performed for osteoclastogenesis assays of three FOA participants expressing OPG-XL and matched healthy controls. Relative activity per osteoclast was calculated by dividing the concentration of CTX-1 by the total number of osteoclasts. Bone resorption was analyzed in cell cultures of two FOA participants expressing OPG-XL and matched healthy controls as previously described (28) with Coomassie Brilliant Blue (Sigma-Aldrich). Pre-defined areas of

each bone slice, covering approximately one fifth of the total area, were analyzed with Image Pro-Plus software (Media Cybernetics).

Histology and immunohistochemistry

Histology was performed as previously described (4). Overall cellular and tissue structure was visualized with hematoxylin-eosin (H&E) staining. Glycosaminoglycans were visualized by staining with 1% Alcian Blue 8-GX (Sigma-Aldrich) and Nuclear Fast red (Sigma-Aldrich). Calcium deposits were visualized with 2% Alizarin Red S (Sigma-Aldrich).

Formation of osteoclasts was assessed after 14 and 21 days of culture on plastic. Osteoclasts were fixed in 4% formaldehyde for 10 min at ambient temperature and stained for tartrate resistant acid phosphatase (TRAcP) using a commercial kit (Leukocyte acid phosphatase kit, Sigma–Aldrich) according to the manufacturer's instructions. Nuclei were visualized with 4'6-diamidino-2-phenylindole dihydrochloride (DAPI, Sigma-Aldrich). Only cells with three or more nuclei were considered osteoclasts. Results are presented as osteoclasts per cm^2 or in nuclei per osteoclast.

Gene expression analysis

For osteoclast assays, RNA was extracted from the different cultures at day 7, 14 and 21. For each individual RNA isolation of neo-cartilage and neo-bone, we pooled two organoids for either OPG-XL or CRISPR/Cas9 repaired (wt) from several independent rounds of differentiations. This generated for neo-cartilage of OPG-XL a total of 5 to 7 datapoints and for wt a total of 9 to 12 datapoints in the gene expression plots. For neo-bone, this generated for OPG-XL and wt a total of respectively 10 to 16 and 7 to 14 datapoints.

A total of 150 ng mRNA was processed with first strand cDNA kit according to manufacturer's protocol (Roche Applied Science). Genes of interest were determined by preamplification with TaqMan preamp master mix (Thermo Fisher Scientific Inc) and subsequent RT-qPCR in triplicate with BiomarkTM 96.96 Dynamic Arrays (Fluidigm) and integrated fluidic circuit (IFC) chip. Quality control of the data was performed as previously described (4). Unsuccessful differentiation experiments defined by the minimum detected expression of *COL2A1* for human primary chondrocytes and BMSCs neo-cartilage, were disregarded. Relative gene expression ($-\Delta$Ct-values) was calculated using levels of glyceraldehyde 3-phosphate dehydrogenase (*GAPDH*) and acidic ribosomal phosphoprotein P0 (*ARP*) as housekeeping genes. The RT-qPCR primers are listed in **Supplementary Table S5**.

Statistical analysis

Generalized estimating equations (GEE) (30) as implemented in IBM SPSS 25.0 software was applied to analyze association between phenotype and genotype. GEE methodology provides a method of analyzing correlated data that otherwise could not be modeled in a generalized linear model. By applying this method, we were able to effectively adjust for familial dependencies of included participants to obtain Betas, standard errors (SE) and P-values for gene expression differences across neo-cartilage and neo-bone (2).

Differences between osteoclast categories defined by the number of nuclei and gene expression were tested using two-way ANOVA and Sidak's multiple comparison test (GraphPad Prism 6.0 software). P-values <0.05 were considered statistically significant.

RESULTS

Carriers of OPG-XL are characterized by severe OA and osteopenia

TNFRSF11B was genotyped in study participants, identifying seven carriers and six non-carriers of OPG-XL among thirteen members of a family with early-onset OA (FOA; **Figure 1**; **Supplementary Table S1**). Whole body DEXA scans showed that bone mineral density (BMD) of non-carriers was similar to that of the general population (**Figure 1C**; **Supplementary Table S2A**). In contrast, carriers of OPG-XL had significantly lower BMD specifically of the femoral neck, narrow neck and total hips, confirming incidence of osteopenia (**Figure 1C**; **Supplementary Table S2B**). No significant difference, however, was observed for lumbar spine BMD. Furthermore, OA features were scored for FOA members based on the semi quantitative MRI OA knee score (MOAKS). This showed that severe osteophytosis, bone marrow lesions (BML), and cysts have significant higher prevalence in carriers of the mutation than in non-carriers (**Supplementary Table S3**). Analysis of the knee radiographs confirmed presence of chondrocalcinosis in three participants expressing OPG-XL. Altogether, this demonstrated that the CCAL1 phenotype in the FOA family is characterized by low BMD and severe cartilage loss, osteophyte formation, and presence of cysts and BML. High mineralization of cartilage was also observed in knee joint of a carrier of the mutation undergoing joint replacement surgery (**Figure 1D**, specific regions with calcified cartilage indicated with dashed line).

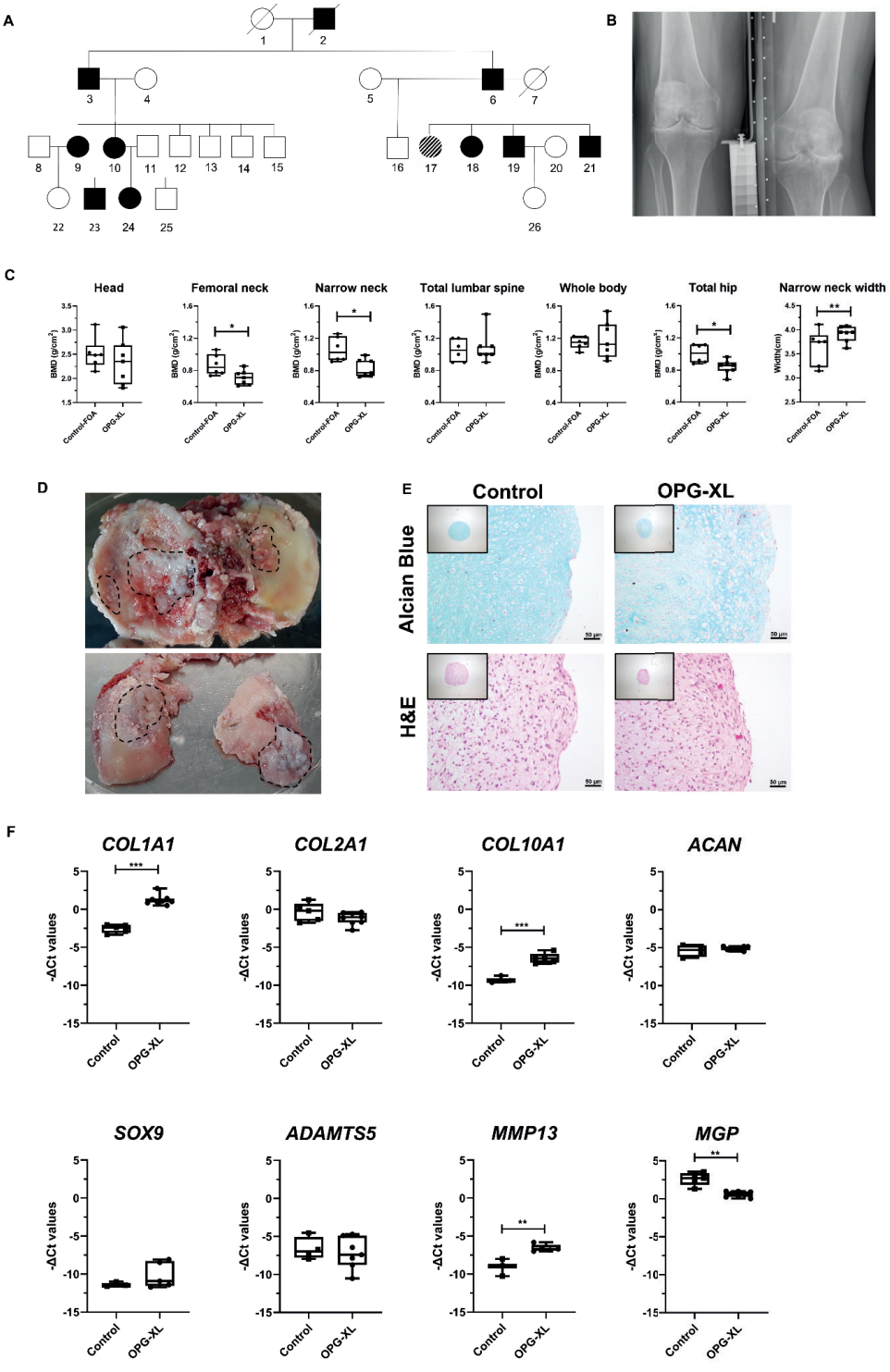
A
1
2
3
4
5
6
7
8
9
10
11
12
13
14
15
16
17
18
19
20
21
22
23
24
25
26
B
C
Head
Femoral neck
Narrow neck
Total lumbar spine
Whole body
Total hip
Narrow neck width
BMD (g/cm²)
Width(cm)
Control-FOA
OPG-XL
D
E
Control
OPG-XL
Alcian Blue
H&E
F
COL1A1
COL2A1
COL10A1
ACAN
SOX9
ADAMTS5
MMP13
MGP
-ΔCt values
Control
OPG-XL

Figure 1. Characterization of early-onset osteoarthritis family. A) Pedigree of early-onset osteoarthritis family (FOA) with the *TNFRSF11B* readthrough mutation (OPG-XL). Squares represent males and circles females (black symbols represent affected individuals; diagonal lines indicate deceased family members). **B**) Knee radiograph of individual no. 9 from the family tree, with severe articular surface destruction. **C**) BMD of family members with and without the OPG-XL mutation as determined by dual energy X-ray absorptiometry scans and corrected for sex, age and BMI (N= 7 OPG-XL family members, N = 6 healthy family members). **D**) Knee joint from patient that underwent replacement surgery (indicated with dashed line regions with severely calcified cartilage). **E**) Alcian blue and H&E staining of neo-cartilage organoids derived from primary chondrocytes of common OA patients and of OPG-XL carrier (day 21 of chondrogenesis; scale bars: 50 mm). **F**) Boxplots for DCt values of matrix genes in neo-cartilage of common OA patients (N = 5 patients, n = 1) and of OPG-XL carrier (N = 1 FOA, n = 8). P-values determined with generalized estimation equation while including every independent gene as dependent variable, BMD as dependent variable, and age, sex, BMI and mutation status as covariate (*P < 0.05; **P < 104 ; ***P < 106). *ACAN*: aggrecan; *ADAMTS5*: a disintegrin and metalloproteinase with thrombospondin motifs; H&E: haematoxylin and eosin; *MGP*: matrix Gla protein; *MMP13*: matrix metallopeptidase 13; OPG-XL: C-terminal extended osteoprotegerin encoded by *TNFRSF11B* readthrough mutation; *SOX9*: SRY-box transcription factor 9.

Primary chondrocytes with OPG-XL deposit hypertrophic neo-cartilage with low glycosaminoglycan content

We first examined, in an established 3D *in vitro* chondrogenesis model of human primary chondrocytes (29) of a carrier of the OPG-XL mutation (N=1 patient, n=8 replicates), formation of neo-cartilage in comparison to primary chondrocytes from participants of the RAAK study undergoing joint replacement surgery (N=5 patients, n=1 replicate). As shown in **Figure 1E**, Alcian blue staining in neo-cartilage with OPG-XL appeared less homogeneous as compared to neo-cartilage deposited by RAAK chondrocytes. Furthermore, H&E staining showed less dense matrix deposition towards the edges of the organoid. Gene expression of common extracellular matrix (ECM) genes and degradation markers highlighted significantly higher expression of *COL1A1*, *COL10A1* and *MMP13* (**Figure 1F**; **Supplementary Table S6**.). Moreover, low MGP expression indicated a higher mineralization in the OPG-XL neo-cartilage organoids. Together, these data indicated deposition of low quality neo-cartilage matrix with a fibrotic (*COL1A1*) and/or hypertrophic (*COL10A1*) and mineralized (*MGP*) phenotype in the presence of OPG-XL.

Neo-cartilage and neo-bone expressing OPG-XL exhibit altered mineralization and fibrotic phenotype

To study effects of OPG-XL on deposition of extracellular matrix in the joint, patient hiPSCs carrying the mutation were generated from skin fibroblasts (**Supplementary Figure S1**), and both neo-cartilage as well as -bone organoids were created from these hiPSCs and two independent isogenic, CRISPR/Cas9-corrected control (wt) hiPSCs. Structure of deposited neo-cartilage ECM was visualized by histological staining with Alcian blue and H&E (**Figure 2A**;

Supplementary Figure S2). This showed ECM deposition across both groups. Matrix however, was more homogeneous in the two isogenic control organoids as compared to organoids from hiPSCs expressing OPG-XL. Additionally, H&E staining visualized fibrotic ECM particularly towards the outer rim of the OPG-XL neo-cartilage organoids.

In line with the histological observations, quantitative gene expression analysis showed no difference between the two isogenic controls (**Figure 2B**, grey- and purple-filled circles in wt boxes). Therefore, samples were analyzed together in comparison to OPG-XL samples which revealed no significant differences in expression levels of *TNFSF11* encoding RANKL, *TNFRSF11A* encoding RANK, nor in expression levels of *TNFRSF11B* in neo-cartilage in the presence of OPG-XL. Fibrotic character of neo-cartilage deposited in presence of OPG-XL was confirmed by significantly higher expression of *COL1A1* and lower expression of the cartilage specific *COL2A1* and aggrecan (*ACAN*). Concurrently, strong upregulation of alkaline phosphatase (*ALPL*) and osteoblast characteristic RUNX family transcription factor 2 (*RUNX2*) were detected together with significantly lower expression of SRY-Box Transcription Factor 9 (*SOX9*). Notably, lower expression of *MGP* was highly significant which was also observed in neo-cartilage deposited by primary chondrocytes with OPG-XL (**Figure 1F**). These data indicated a strong shift in cartilage metabolism towards mineralization and transdifferentiation towards osteoblasts. This was in contrast with lower expression levels of Secreted Phosphoprotein 1 (*SPP1*) and matrix metallopeptidase 13 (*MMP13*).

Structure of deposited neo-bone ECM was visualized by histological staining with Alizarin red and H&E **(Figure 2A**; **Supplementary Figure S2)**. Alizarin red staining was more intense and more homogeneously distributed in the OPG-XL organoids compared to isogenic controls. In the control group, H&E showed a higher concentration of cells within the core of the organoid and an outer rim characterized by fibrosis.

In line with the findings in cartilage organoids, quantitative gene expression analysis of neo-bone showed no significant differences in levels of *TNFRSF11B* and *TNFRSF11A* expression. Unlike neo-cartilage, neo-bone carrying the OPG-XL mutation did show lower expression of *TNFSF11* (**Figure 2B**; **Table 1**; **Supplementary Figure S3**). Moreover, neo-bone expressing OPG-XL had significantly higher expression of *COL1A1* and *COL10A1*, but particularly of *DIO2*. Altogether, results indicate that both neo-cartilage and neo-bone ECM in the presence of OPG-XL is characterized by increased fibrosis and strong mineralization, respectively, indicating a modulatory role for OPG in cartilage and bone formation.

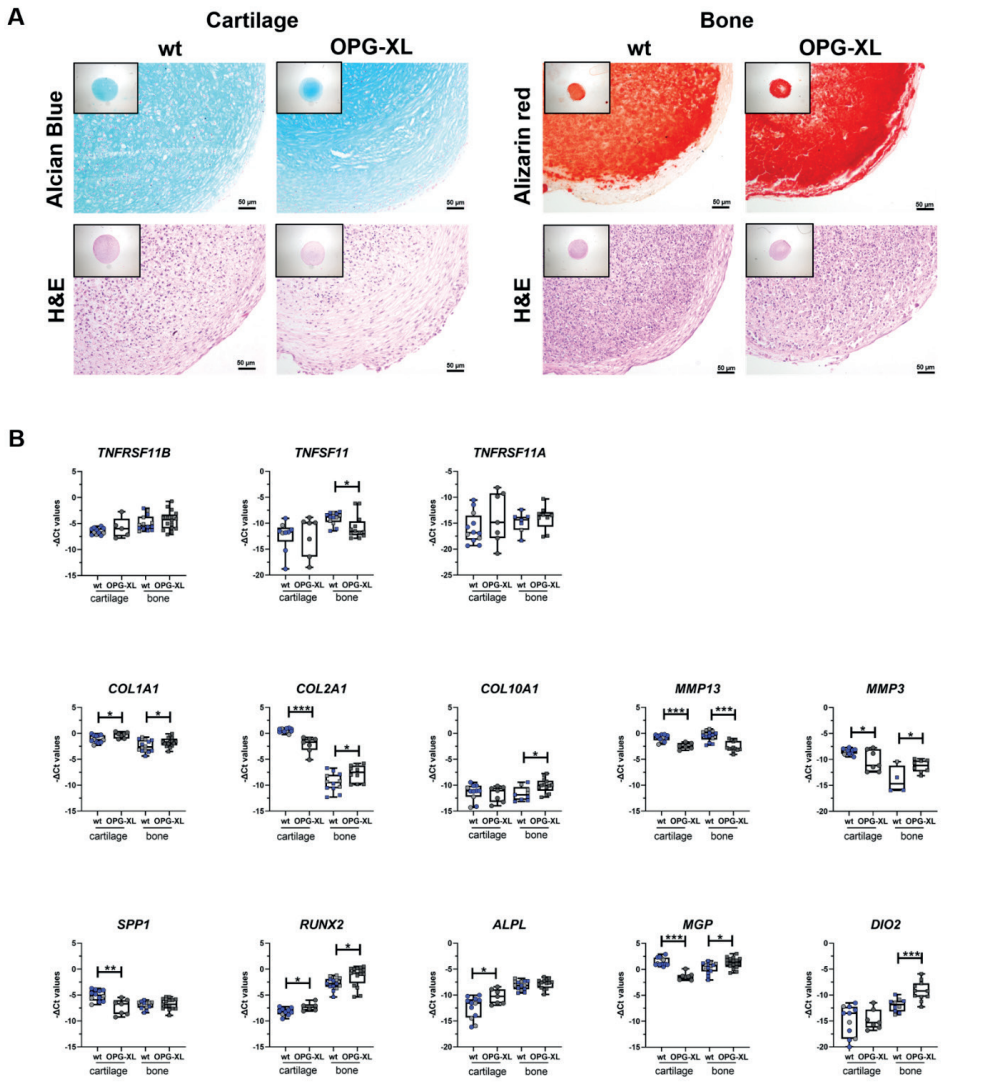

Figure 2. Characterization of OPG-XL neo-cartilage and neo-bone organoids. Alcian blue, Alizarin red and H&E staining of neo-cartilage and neo-bone. **B**) Boxplots for -ΔCt values of relevant genes for CRISPR/Cas9 control (WT) and OPG-XL organoids following 6 weeks of chondrogenesis with additional 2 weeks of osteogenesis to generate neo-bone (scale bars: 50 mm; neo-cartilage: WT n = 9–12 and OPG-XL n = 5–7 samples; neo-bone: WT n = 7–14 and OPG-XL n = 10–16 samples). P-values determined with generalized estimation equation while including every independent gene as dependent variable, and mutation status as covariate (*P < 0.05; **P < 104 ; ***P < 106). *ALPL*: alkaline phosphatase; *DIO2*: type 2 deiodinase; H&E: haematoxylin and eosin; *MGP*: matrix Gla protein; *MMP3*: matrix metallopeptidase 3; *MMP13*: matrix metallopeptidase 13; OPG-XL: C-terminal extended osteoprotegerin encoded by *TNFRSF11B* readthrough mutation; *RUNX2*: RUNX family transcription factor 2; *SPP1*: secreted phosphoprotein 1; *TNFSF11*: gene encoding RANK ligand; *TNFRSF11A*: gene encoding RANK; *TNFRSF11B*: gene encoding osteoprotegering or OPG.

Table 1. Gene expression analyses of neo-cartilage and neo-bone organoids.

Neo-Cartilage									
Extracellular matrix					Mineralization				
Genes	**FD**	**Beta**	**SE**	**P value[a]**	**Genes**	**FD**	**Beta**	**SE**	**P value[a]**
COL1A1	**1.7**	**0.8**	**0.3**	**$7.4x10^{-3}$**	**SPP1**	**-4.6**	**-2.2**	**0.6**	**$2.0x10^{-4}$**
COL2A1	**-6.7**	**-2.8**	**0.5**	**$3.9x10^{-7}$**	**RUNX2**	**1.9**	**0.9**	**0.4**	**$1.0x10^{-2}$**
COL10A1	-1.2	-0.3	0.7	$6.4x10^{-1}$	**ALPL**	**4.4**	**2.1**	**0.8**	**$5.9x10^{-3}$**
MMP13	**-2.4**	**-1.6**	**0.3**	**$1.4x10^{-8}$**	**MGP**	**-7.1**	**-2.8**	**0.3**	**$1.6x10^{-17}$**
MMP3	**-3.4**	**-1.8**	**0.7**	**$1.5x10^{-2}$**	POSTN	1.1	0.2	0.3	$5.2x10^{-1}$
TNFRSF11B	1.6	0.7	0.8	$4.0x10^{-1}$	ASPN	1.0	0.0	0.3	$9.5x10^{-1}$
TNFRSF11A	1.8	2.0	1.9	$2.9x10^{-1}$	DIO2	1.2	0.3	1.1	$8.0x10^{-1}$
TNFRSF11	1.0	0.1	1.6	$9.7x10^{-1}$	ANKH	-1.2	-0.2	0.5	$6.9x10^{-1}$
ACAN1	**-3.9**	**-2.0**	**0.8**	**$1.5x10^{-2}$**					
SOX9	**-2.0**	**-1.0**	**0.3**	**$4.5x10^{-3}$**					
COMP	-1.2	-0.3	0.2	$1.8x10^{-1}$					
ADAMTS5	1.6	0.6	1.1	$5.6x10^{-1}$					
SMAD3	**-2.7**	**-1.4**	**0.4**	**$4.0x10^{-4}$**					
Neo-bone									
Extracellular matrix					Mineralization				
Genes	**FD**	**Beta**	**SE**	**P value[a]**	**Genes**	**FD**	**Beta**	**SE**	**P value[a]**
COL1A1	**1.7**	**0.7**	**0.4**	**$3.9x10^{-2}$**	SPP1	1.1	0.2	0.3	$5.8x10^{-1}$
COL2A1	**3.3**	**1.7**	**0.7**	**$1.2x10^{-2}$**	**RUNX2**	**2.8**	**1.5**	**0.6**	**$7.7x10^{-3}$**
COL10A1	**4.8**	**1.5**	**0.6**	**$5.6x10^{-3}$**	ALPL	1.2	0.3	0.3	$3.4x10^{-1}$
MMP13	**-3.3**	**-2.1**	**0.4**	**$7.8x10^{-9}$**	**MGP**	**1.9**	**0.9**	**0.4**	**$1.2x10^{-2}$**
MMP3	**-14.9**	**2.6**	**1.2**	**$2.8x10^{-2}$**	POSTN	-1.4	-0.5	0.5	$3.14x10^{-1}$
TNFRSF11B	1.5	0.6	0.6	$3.3x10^{-1}$	**ASPN**	**-3.6**	**-1.8**	**0.5**	**$1.4x10^{-4}$**
TNFRSF11A	1.8	0.9	1.0	$3.8x10^{-1}$	**DIO2**	**6.6**	**2.7**	**0.7**	**$3.5x10^{-5}$**
TNFSF11	**-3.2**	**-1.7**	**0.7**	**$2.0x10^{-2}$**	IL11	1.6	0.7	0.5	$1.8x10^{-1}$
					SOST	**2.9**	**1.5**	**0.7**	**$3.5x10^{-2}$**

Results presented are the average of seven samples for neo-cartilage and 16 samples for neo-bone in OPG-XL carriers compared with 12 samples for neo-cartilage and 14 samples for neo-bone in CRISPR/Cas9-corrected controls (WT) at week 6 following chondrogenesis and additional 2 weeks following osteogenesis. P-values determined with generalized estimation equation while including every independent gene as dependent variable, and mutation status as covariate (P-values >0.05 are indicated in bold). FD: fold difference.

Restrained osteoclastogenesis and large polykaryons of monocytes from FOA patients expressing OPG-XL

Given that OPG plays a key role in osteoclast formation, osteoclastogenesis assays were performed with monocytes from six carriers of OPG-XL mutation and six healthy controls (**Figure 3A**). The number of osteoclasts and their respective nuclei were determined at day 14 and day 21 of culture (**Supplementary Table S7**). As shown in **Figure 3B** and **Supplementary Table S7**, the total number of osteoclasts (cells with >3 nuclei) formed at day 14 in OPG-XL (n=90) is delayed relative to controls (n=296). At day 21, however, we showed a significant accumulation of osteoclasts with high number of nuclei formed in OPG-XL (39% >6 nuclei) compared to controls (15% >6 nuclei; **Figure 3C**; **Supplementary Table S7**). Together, these data indicate that after initial restrained osteoclastogenesis, a relative larger fraction of osteoclasts with large number of nuclei accumulate in the presence of OPG-XL as compared to controls.

A

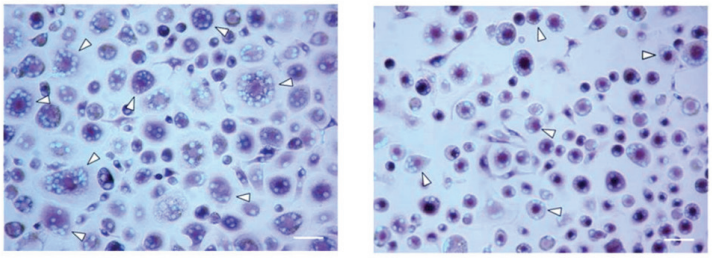

B

TRAcP positive cells/cm² at day 14			
Nuclei/osteoclast [a]	**Controls [b]**	**OPG-XL [b]**	**P value [c]**
3-5	263 (89%)	86 (96%)	$5.9x10^{-2}$
6-10	30 (10%)	4 (4%)	$9.5x10^{-2}$
10-20	3 (1%)	0	ND
>20	0	0	ND
Total	296	90	

TRAcP positive cells/cm² at day 21			
Nuclei/osteoclast [a]	**Controls [b]**	**OPG-XL [b]**	**P value [c]**
3-5	644 (85%)	290 (61%)	$2.5x10^{-21}$
6-10	94 (12%)	114 (24%)	$1.1x10^{-7}$
10-20	13 (2%)	53 (11%)	$6.8x10^{-13}$
>20	6 (1%)	16 (3%)	$1.2x10^{-3}$
Total	757	473	

[a] Strata of osteoclasts according to the number of nuclei per osteoclast. [b] Average number of osteoclasts from N = 6 OPG-XL carriers and N = 6 sex- and age-matched controls; 2–3 replicates each were counted. [c] *P*-value for each stratum was determined with $\chi 2$ test relative to total number of osteoclasts in all other strata.

Figure 3. Characterization of osteoclastogenesis. A) Representative TRAcP staining of osteoclasts generated from monocytes of OPG-XL carriers and sex- and agematched controls after 21 days of culture with M-CSF and RANKL (Scale bar = 200 μm). **B**) Osteoclasts were counted and separated according to the number of nuclei per osteoclast at day 14 and day 21. OPG-XL: C-terminal extended osteoprotegerin encoded by *TNFRSF11B* readthrough mutation; RANKL: RANK ligand; TRAcP: Tartrate-resistant acid phosphatase.

Osteoclasts expressing OPG-XL display similar bone resorptive activity as compared to controls

Following morphological characterization of osteoclasts, resorptive activity was assessed. To that end, formation of resorption pits by osteoclasts generated from controls and from carriers of OPG-XL was determined. As shown in **Figure 4**, despite lower numbers of osteoclasts in the presence of OPG-XL, overall bone resorption was comparable, with at least equal surface areas of resorption pits after 21 days (**Figure 4A**) and amounts of CTX-I released at days 7, 14, and 21 (**Figure 4B-D**). These data indicate that, despite the fact that less osteoclasts develop in the presence of OPG-XL, the total bone resorption activity was comparable to controls.

Finally, well-known markers of osteoclast bone resorption activity were analyzed by RT-qPCR. As shown in **Figure 4E** and **Table 2**, at day 21 OPG-XL-expressing osteoclasts showed significantly higher levels of *NFATc1* (Nuclear factor of activated T-cells, cytoplasmic 1), *CTSK* (Cathepsin K), *TRAcP* (Tartrate-resistant acid phosphatase) and *DC-STAMP* (Dendrocyte Expressed Seven Transmembrane Protein). This suggests that monocytes carrying the OPG-XL mutation, despite an initial delay in osteoclastogenesis, are prone to differentiate towards osteoclasts with potential for higher bone resorption activity based on gene expression levels.

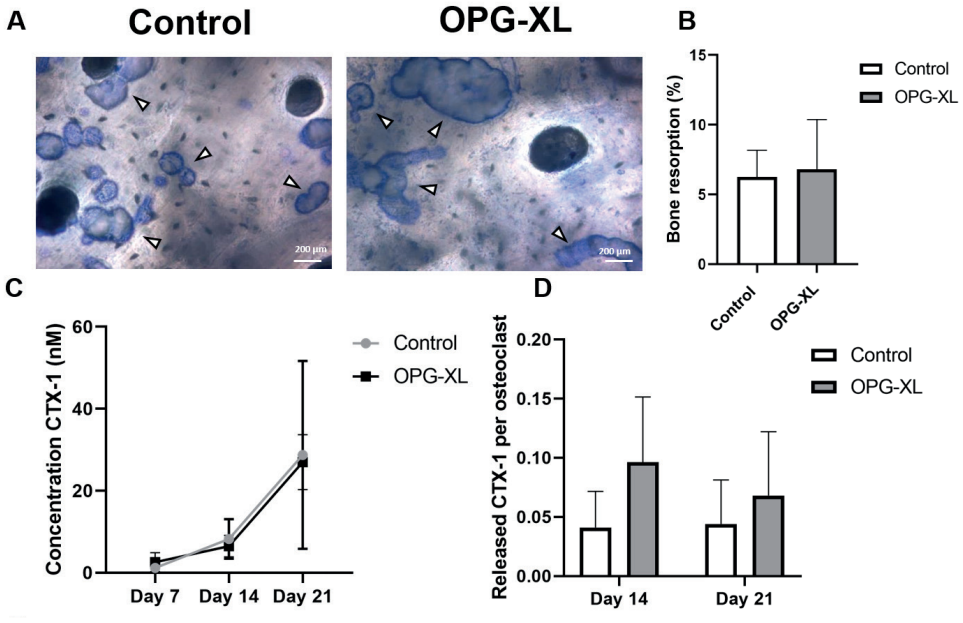

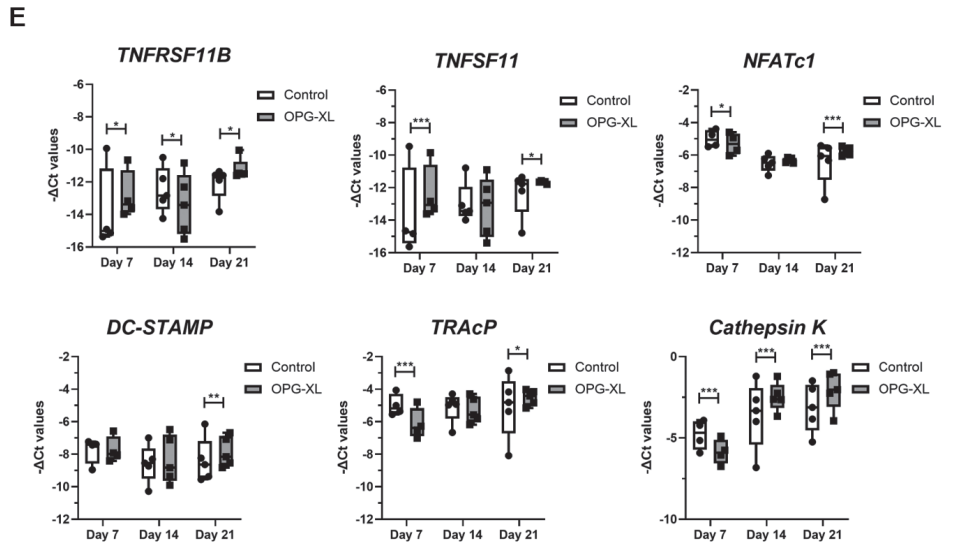

Figure 4. Bone resorption and gene expression for osteoclasts from controls and OPG-XL carriers. **A**) Representative image of bone resorption pits formed by osteoclasts from control and OPG-XL carrier on slices of human tibia bone after 21 days of culture (scale bars: 200 μm). **B**) Percentage of bone resorption for controls (N = 2) and OPG-XL carriers (N = 2). **C**) Concentration of CTX-1 (nM) in conditioned medium after 7, 14 and 21 days of culture (controls and OPG-XL carriers N = 3). **D**) CTX-1 release in conditioned medium per osteoclast at 14 and 21 days of culture (controls N = 3 and OPG-XL carriers N = 3). **E**) Boxplots for -ΔCt values of genes related to osteoclast formation and activity (n = 2–3 replicates from 4–5 controls and OPG-XL carriers). P-values determined with two-way ANOVA with Sidak's multiple comparison analysis (*$P < 0.05$; **$P < 10^{-4}$; ***$P < 10^{-6}$). *CTX-1*: C-terminal telopeptide of type 1 collagen; *DC-STAMP*: endrocyte Expressed Seven Transmembrane Protein; *NFATc1*: Nuclear factor of activated T-cells, cytoplasmic 1; OPG-XL: C-terminal extended osteoprotegerin encoded by *TNFRSF11B* readthrough mutation; *TNFSF11*: gene encoding RANK ligand; *TNFRSF11B*: gene encoding osteoprotegerin or OPG; *TRAcP*: Tartrate-resistant acid phosphatase.

Table 2. Gene expression analyses of osteoclasts from OPG-XL carriers and sex- and age-matched controls.

Markers of osteoclast activity					
	FD	**P value**		**FD**	**P value**
TNFRSF11B			***DC-STAMP***		
Day 7	**2.0**	**$1.7x10^{-2}$**	Day 7	1.0	$9.9x10^{-1}$
Day 14	**-1.9**	**$1.5x10^{-2}$**	Day 14	1.2	$9.5x10^{-2}$
Day 21	**1.8**	**$2.8x10^{-2}$**	**Day 21**	**1.5**	**$1.0x10^{-4}$**
TNFSF11			**TRAcP**		
Day 7	**2.4**	**$1.0x10^{-4}$**	**Day 7**	**-2.2**	**$1.0x10^{-4}$**
Day 14	-1.2	$6.4x10^{-1}$	Day 14	-1.1	$5.7x10^{-1}$
Day 21	**1.6**	**$1.6x10^{-2}$**	**Day 21**	**1.5**	**$6.2x10^{-3}$**
NFATc1			***CTSK***		
Day 7	**-1.3**	**$1.2x10^{-2}$**	**Day 7**	**-2.1**	**$1.0x10^{-4}$**
Day 14	1.1	$1.2x10^{-1}$	**Day 14**	**2.2**	**$1.0x10^{-4}$**
Day 21	**1.6**	**$1.0x10^{-4}$**	**Day 21**	**2.1**	**$1.0x10^{-4}$**

[a]Results presented are the average of $n = 2–3$ replicates from $N = 4–5$ OPG-XL carriers compared with age- and sex-matched controls. *P*-values determined with two-way ANOVA with Sidak's multiple comparison analysis (P-values > 0.05 are indicated in bold). FD: fold difference; OPG-XL: C-terminal extended osteoprotegerin encoded by *TNFRSF11B* readthrough mutation.

DISCUSSION

In the current study we explored the mechanism by which OPG-XL causes the characteristic bidirectional phenotype of subchondral bone turnover accompanied by cartilage mineralization in CCAL1 patients. Notably, OPG-XL displaying 19 additional amino acids at the C-terminal end, was previously found to hamper the formation of a stable HS-OPG-RANKL complex on the osteoblast membrane, (17) permitting RANKL mediated osteoclastogenesis in a murine model (11). Here we show that human osteoclastogenesis with monocytes from OPG-XL carriers relative to sex- and age-matched controls after an initial delay, indeed have enhanced osteoclastogenesis towards prominent large and active osteoclasts. By further characterization of OPG-XL by employing hiPSCs from a carrier of the mutation and two isogenic CRISPR/Cas9-corrected controls in cartilage and bone organoids, we demonstrated for the first time that, likely due to interference with RANKL-HS-OPG, the mutation at the CCAL1 locus directly affects healthy osteoblast and chondrocyte states towards mineralization via respectively *DIO2* and *MGP* functions. The fact that OPG/RANKL as well as *DIO2* (29) and *MGP* (2, 31) are intrinsically involved in joint tissue (patho)physiology might indicate a link to common age-related osteoarthritis.

The hiPSC-derived neo-cartilage tissue deposited by OPG-XL chondrocytes, relative to isogenic controls, revealed a fibrotic histological phenotype with marked downregulation of *COL2A1:COL1A1* ratio and most notable, downregulation of *MGP* expression. *MGP* is a well-known inhibitor of ectopic bone formation (5) and a robust OA risk gene (24, 31) with the risk allele associated towards lower gene expression levels (2, 31). Hence, our data, showing lower expression of *MGP* in OPG-XL neo-cartilage organoids, suggest that OPG-XL directly affects propensity of chondrocytes to enter a mineralized OA state. On a different note, we showed that in OPG-XL neo-cartilage organoids the OPG/RANKL/RANK triad was not changed.

Neo-osseous tissue deposited by osteoblasts from hiPSCs carrying the mutation relative to their isogenic controls did display high calcification as reflected by the prominent Alizarin red staining concurrent with notable high expression of *DIO2*. *DIO2*, encoding type 2 deiodinase enzyme, is essentially facilitating bone formation and mineralization (32). Together, results of our human OPG-XL cartilage and bone organoids demonstrates that the mutation directly affects chondrocyte and osteoblast gene expression profiles marking matrix mineralization processes. We hypothesize that this is due to the impaired binding of OPG with HS, likely in interaction with RANKL as recently shown (11). Since the prominent Alizarin red staining of neo-osseous tissue, concurrent with *DIO2* upregulation could explain the extensive phenotypic foci of calcified cartilage observed in affected articular cartilage tissue of CCAL1 family members, we hypothesize that the chondrocalcinosis observed in OPG-XL carriers is likely not preceding OA onset in cartilage but arises merely during ongoing OA pathophysiology i.e. when chondrocytes have a tendency to undergo trans-differentiation to osteoblast (33).

By performing osteoclastogenesis assays of OPG-XL carriers relative to age- and sex-matched controls we showed that, although significantly lower in number, osteoclastogenesis in OPG-XL carriers resulted in high nucleated osteoclasts (**Figure 3**). These multi-nuclear osteoclasts appear at least equally active as controls as demonstrated by the comparable resorbed bone surface and released levels of CTX-I (**Figure 4**). The fact that we were able to quantify the resorption pits only for 2 donors and controls has likely resulted in limited statistical power to detect small differences. This hypothesis could hence explain the bidirectional phenotype of the OPG-XL carriers characterized by higher cartilage mineralization and osteopenia. A similar case was previously reported by Zhang et al (34), where MGP knock out mice have a characteristic phenotype of premature bone mineralization and osteopenia. Since RANKL was found to induce osteoclast fusion whereas OPG blocked fusion of highly mobile osteomorphs, (15) it is tempting to link the role of immobilized OPG on

the surface of osteoblasts to *in vivo* recycling of osteoclasts (35). Nevertheless, our study does not allow to distinguish whether the OPG-XL mutation results in highly nucleated and active osteoclasts due to enhanced RANKL availability or due to dysfunctional blocking of osteomorph fusion.

Among genes significantly changed in the presence of OPG-XL we observed that *MMP13* was higher in the primary chondrocytes while it was lower in the iPSC-derived chondrocytes. This suggests that *MMP13* itself is not directly related to the changes resulting from OPG-XL, but rather, that the effect results from individual variation and/or differences in the maturity of neo-cartilage derived from hiPSCs as compared to that of primary chondrocytes.

By precise genetic engineering of hiPS cells derived from affected CCAL1 family members, while applying established differentiation protocols towards human biomimetic cartilage and osseous organoids, (36) we could study in multiple biological replicates how expression of OPG-XL could result in the characteristic bidirectional phenotype of subchondral bone turnover accompanied by cartilage mineralization. Strength of using isogenic controls is that this allows to study unbiased effects of the mutation, independent of variation between family members such as genetics, sex or age. As such, we are confident that our approach was able to create reliable data highly translating to human *in vivo* situation while complying to the societal need to reduce animal studies (37, 38). A potential drawback of our study is that we were not able to model direct interaction between cells populating cartilage and bone; chondrocytes, osteoblast and osteoclasts. In this context, using the isogenic pairs of our patient-derived hiPSCs in human joint-on-chip models, currently being developed, could further address the molecular mechanism underlying the bi-directional effect OPG on hard and soft tissues (39, 40).

In conclusion, our data demonstrated that expression of OPG-XL in human cartilage and bone is not only enhancing RANKL-induced osteoclastogenesis but also directly affecting chondrocyte and osteoblast states towards matrix mineralization via functions of respectively *MGP* and *DIO2*. We advocate that the bidirectional phenotype of subchondral bone turnover accompanied by cartilage mineralization is a characteristic process that occurs in CCAL1 patients at early ages but which can be extrapolated to common age related OA patients. Vice versa, our data suggest that in cartilage, proper binding of OPG to HS on chondrocytes intrinsically contributes to a healthy unmineralized tissue state while in bone it supports the steady state turnover with adaptive activity involving osteoblasts and osteoclasts.

Acknowledgements

We thank members of the early-onset family and all the participants of the RAAK study. The LUMC has and is supporting the RAAK study. We thank all the members of our group for valuable discussion and feedback. We also thank Enrike van der Linden, Demiën Broekhuis, Peter van Schie, Shaho Hasan, Maartje Meijer, Daisy Latijnhouwers and Geert Spierenburg for collecting the RAAK material, and Luuk Ciere and Ankita Das for their support in the disease model generation. We thank Valeria Orlova for expert suggestions regarding differentiation of hiPSCs, and the Sequence Analysis Support Core (SASC) of the Leiden University Medical Center for their support.

Funding

Research leading to these results has received funding from the Dutch Arthritis Society (DAF-16-1-406 and DAF-16-1-405), and the Dutch Scientific Research council NWO/ZonMW VICI scheme (nr 91816631/528). This work was partly supported by grants from Marie Curie Initial Training Network (Euroclast, FP7-People-2013-ITN: #607447). Data is generated within the scope of the Medical Delta programs Regenerative Medicine 4D and Improving Mobility with Technology.

Disclosure of potential conflicts of interest

None declared.

Data availability statement

The data that support the funding of this study are available from the corresponding author upon request.

Ethics approval and consent to participate

The Medical Ethics Committee of the LUMC gave approval for the RAAK study (P08.239 and P19.013), the familial OA (FOA) study (P12-256), and for generation of hiPSCs from skin fibroblasts of healthy donors (P13.080). Informed consent was obtained from all participants and donors in our manuscript.

REFERENCES

1. Findlay DM, Kuliwaba JS. Bone-cartilage crosstalk: a conversation for understanding osteoarthritis. Bone Res. 2016;4:16028-40.
2. Houtman E, Coutinho de Almeida R, Tuerlings M, Suchiman HED, Broekhuis D, Nelissen R, et al. Characterization of dynamic changes in Matrix Gla Protein (MGP) gene expression as function of genetic risk alleles, osteoarthritis relevant stimuli, and the vitamin K inhibitor warfarin. Osteoarthritis Cartilage. 2021;29(8):1193-1202.
3. Vassalle C, Mazzone A. Bone loss and vascular calcification: A bi-directional interplay? Vascul Pharmacol. 2016;86:77-86.
4. Bucay N, Sarosi I, Dunstan CR, Morony S, Tarpley J, Capparelli C, et al. osteoprotegerin-deficient mice develop early onset osteoporosis and arterial calcification. Genes Dev. 1998;12(9):1260-8.
5. Luo G, Ducy P, McKee MD, Pinero GJ, Loyer E, Behringer RR, et al. Spontaneous calcification of arteries and cartilage in mice lacking matrix GLA protein. Nature. 1997;386(6620):78-81.
6. Theoleyre S, Wittrant Y, Tat SK, Fortun Y, Redini F, Heymann D. The molecular triad OPG/RANK/RANKL: involvement in the orchestration of pathophysiological bone remodeling. Cytokine Growth Factor Rev. 2004;15(6):457-75.
7. Kiechl S, Werner P, Knoflach M, Furtner M, Willeit J, Schett G. The osteoprotegerin/RANK/RANKL system: a bone key to vascular disease. Expert Rev Cardiovasc Ther. 2006;4(6):801-11.
8. Tschiderer L, Willeit J, Schett G, Kiechl S, Willeit P. Osteoprotegerin concentration and risk of cardiovascular outcomes in nine general population studies: Literature-based meta-analysis involving 26,442 participants. PLOS ONE. 2017;12(8):e0183910.
9. Ramos YF, Bos SD, van der Breggen R, Kloppenburg M, Ye K, Lameijer EW, et al. A gain of function mutation in *TNFRSF11B* encoding osteoprotegerin causes osteoarthritis with chondrocalcinosis. Ann Rheum Dis. 2015;74(9):1756-62.
10. Baldwin CT, Farrer LA, Adair R, Dharmavaram R, Jimenez S, Anderson L. Linkage of early-onset osteoarthritis and chondrocalcinosis to human chromosome 8q. Am J Hum Genet. 1995;56(3):692-7.
11. Mitton-Fitzgerald E, Gohr CM, Williams CJ, Ortiz A, Mbalaviele G, Rosenthal AK. Effects of the *TNFRSF11B* Mutation Associated With Calcium Pyrophosphate Deposition Disease in Osteoclastogenesis in a Murine Model. Arthritis & Rheumatology. 2021;73(8):1543-9.
12. Williams CJ, Qazi U, Bernstein M, Charniak A, Gohr C, Mitton-Fitzgerald E, et al. Mutations in osteoprotegerin account for the CCAL1 locus in calcium pyrophosphate deposition disease. Osteoarthritis Cartilage. 2018;26(6):797-806.
13. Meulenbelt I, Bijkerk C, Breedveld FC, Slagboom PE. Genetic linkage analysis of 14 candidate gene loci in a family with autosomal dominant osteoarthritis without dysplasia. J Med Genet. 1997;34(12):1024-7.
14. Boyce BF, Xing L. Functions of RANKL/RANK/OPG in bone modeling and remodeling. Arch Biochem Biophys. 2008;473(2):139-46.
15. McDonald MM, Khoo WH, Ng PY, Xiao Y, Zamerli J, Thatcher P, et al. Osteoclasts recycle via osteomorphs during RANKL-stimulated bone resorption. Cell. 2021;184(5):1330-47.e13.
16. Li M, Yang S, Xu D. Heparan Sulfate Regulates the Structure and Function of Osteoprotegerin in Osteoclastogenesis. The Journal of biological chemistry. 2016;291(46):24160-71.
17. Li M, Xu D. Antiresorptive activity of osteoprotegerin requires an intact heparan sulfate-binding site. Proceedings of the National Academy of Sciences. 2020;117(29):17187-94.
18. Abhishek A, Doherty S, Maciewicz R, Muir K, Zhang W, Doherty M. Association between low cortical bone mineral density, soft-tissue calcification, vascular calcification and chondrocalcinosis: a case-control study. Ann Rheum Dis. 2014;73(11):1997-2002.
19. Coutinho de Almeida R, Ramos YFM, Mahfouz A, den Hollander W, Lakenberg N, Houtman E, et al. RNA sequencing data integration reveals an miRNA interactome of osteoarthritis cartilage. Ann Rheum Dis. 2019;78(2):270-7.

20. Ramos YF, den Hollander W, Bovee JV, Bomer N, van der Breggen R, Lakenberg N, et al. Genes involved in the osteoarthritis process identified through genome wide expression analysis in articular cartilage; the RAAK study. PLoS One. 2014;9(7):e103056.
21. den Hollander W, Ramos YF, Bomer N, Elzinga S, van der Breggen R, Lakenberg N, et al. Transcriptional associations of osteoarthritis-mediated loss of epigenetic control in articular cartilage. Arthritis Rheumatol. 2015;67(8):2108-16.
22. Ijiri K, Zerbini LF, Peng H, Otu HH, Tsuchimochi K, Otero M, et al. Differential expression of GADD45beta in normal and osteoarthritic cartilage: potential role in homeostasis of articular chondrocytes. Arthritis Rheum. 2008;58(7):2075-87.
23. Tuerlings M, van Hoolwerff M, Houtman E, Suchiman E, Lakenberg N, Mei H, et al. RNA Sequencing Reveals Interacting Key Determinants of Osteoarthritis Acting in Subchondral Bone and Articular Cartilage: Identification of IL11 and CHADL as Attractive Treatment Targets. Arthritis Rheumatol. 2021;73(5):789-99.
24. Boer CG, Hatzikotoulas K, Southam L, Stefánsdóttir L, Zhang Y, Coutinho de Almeida R, et al. Deciphering osteoarthritis genetics across 826,690 individuals from 9 populations. Cell. 2021;184(18):4784-818.e17.
25. Rodriguez Ruiz A, Dicks A, Tuerlings M, Schepers K, van Pel M, Nelissen R, et al. Cartilage from human-induced pluripotent stem cells: comparison with neo-cartilage from chondrocytes and bone marrow mesenchymal stromal cells. Cell Tissue Res. 2021;386(2):309-320.
26. Dambrot C, van de Pas S, van Zijl L, Brandl B, Wang JW, Schalij MJ, et al. Polycistronic lentivirus induced pluripotent stem cells from skin biopsies after long term storage, blood outgrowth endothelial cells and cells from milk teeth. Differentiation. 2013;85(3):101-9.
27. Sprangers S, Schoenmaker T, Cao Y, Everts V, de Vries TJ. Different Blood-Borne Human Osteoclast Precursors Respond in Distinct Ways to IL-17A. J Cell Physiol. 2016;231(6):1249-60.
28. de Vries TJ, Schoenmaker T, Beertsen W, van der Neut R, Everts V. Effect of CD44 deficiency on in vitro and in vivo osteoclast formation. J Cell Biochem. 2005;94(5):954-66.
29. Bomer N, denHollander W, Ramos YF, Bos SD, van der Breggen R, Lakenberg N, et al. Underlying molecular mechanisms of DIO2 susceptibility in symptomatic osteoarthritis. Ann Rheum Dis. 2015;74(8):1571-9.
30. Zeger SL, Liang KY. Longitudinal data analysis for discrete and continuous outcomes. Biometrics. 1986;42(1):121-30.
31. den Hollander W, Boer CG, Hart DJ, Yau MS, Ramos YFM, Metrustry S, et al. Genome-wide association and functional studies identify a role for matrix Gla protein in osteoarthritis of the hand. Ann Rheum Dis. 2017;76(12):2046-53.
32. Bassett JH, Boyde A, Howell PG, Bassett RH, Galliford TM, Archanco M, et al. Optimal bone strength and mineralization requires the type 2 iodothyronine deiodinase in osteoblasts. Proc Natl Acad Sci U S A. 2010;107(16):7604-9.
33. Zhou X, von der Mark K, Henry S, Norton W, Adams H, de Crombrugghe B. Chondrocytes transdifferentiate into osteoblasts in endochondral bone during development, postnatal growth and fracture healing in mice. PLoS genetics. 2014;10(12):e1004820.
34. Zhang Y, Zhao L, Wang N, Li J, He F, Li X, et al. Unexpected Role of Matrix Gla Protein in Osteoclasts: Inhibiting Osteoclast Differentiation and Bone Resorption. Mol Cell Biol. 2019;39(12).
35. Jansen ID, Vermeer JA, Bloemen V, Stap J, Everts V. Osteoclast fusion and fission. Calcif Tissue Int. 2012;90(6):515-22.
36. Takahashi K, Tanabe K, Ohnuki M, Narita M, Ichisaka T, Tomoda K, et al. Induction of pluripotent stem cells from adult human fibroblasts by defined factors. Cell. 2007;131(5):861-72.
37. Bédard P, Gauvin S, Ferland K, Caneparo C, Pellerin È, Chabaud S, et al. Innovative Human Three-Dimensional Tissue-Engineered Models as an Alternative to Animal Testing. Bioengineering (Basel). 2020;7(3):115-55.
38. Goldstein DB, Allen A, Keebler J, Margulies EH, Petrou S, Petrovski S, et al. Sequencing studies in human genetics: design and interpretation. Nat Rev Genet. 2013;14(7):460-70.

39. Ma H-P, Deng X, Chen D-Y, Zhu D, Tong J-L, Zhao T, et al. A microfluidic chip-based co-culture of fibroblast-like synoviocytes with osteoblasts and osteoclasts to test bone erosion and drug evaluation. R Soc Open Sci. 2018;5(9):180528-40.
40. Wu Q, Liu J, Wang X, Feng L, Wu J, Zhu X, et al. Organ-on-a-chip: recent breakthroughs and future prospects. Biomed Eng Online. 2020;19(1):9-28.

Supplementary figures:

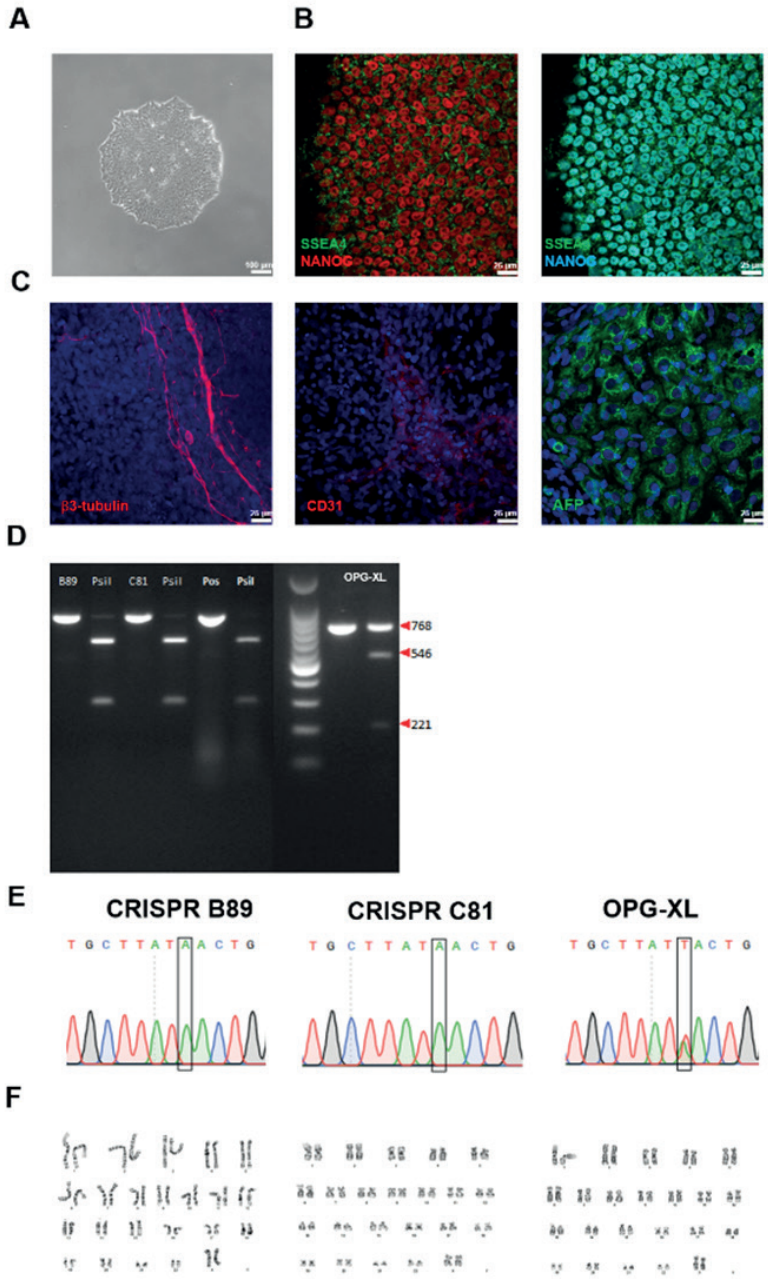

Supplementary Figure S1. Characterization of generated OPG-XL hiPSCs and CRISPR/Cas9-corrected clonal screening. A) Bright field microscopy image of a representative OPG-XL mutated hiPSC colony. **B**) Immunofluorescent staining for NANOG, SSEA-4, and OCT3/4 confirming pluripotency. **C**) Expression of β3-Tubulin, CD31, and AFP upon spontaneous differentiation into

the three different lineages (ectoderm, mesoderm and endoderm, respectively). Nuclei are stained with Dapi (blue). **D**) Clonal screening for OPG-XL repaired mutation by genomic PCR followed by PsiI digestion. Patient DNA shows three bands after PsiI digestion, whereas repaired clones B89 (gRNA1) and C81 (gRNA2) together with the positive control show two bands. **E**) Sanger sequencing and **F**) karyotyping of 2 corrected clones and OPG-XL hiPSC line.

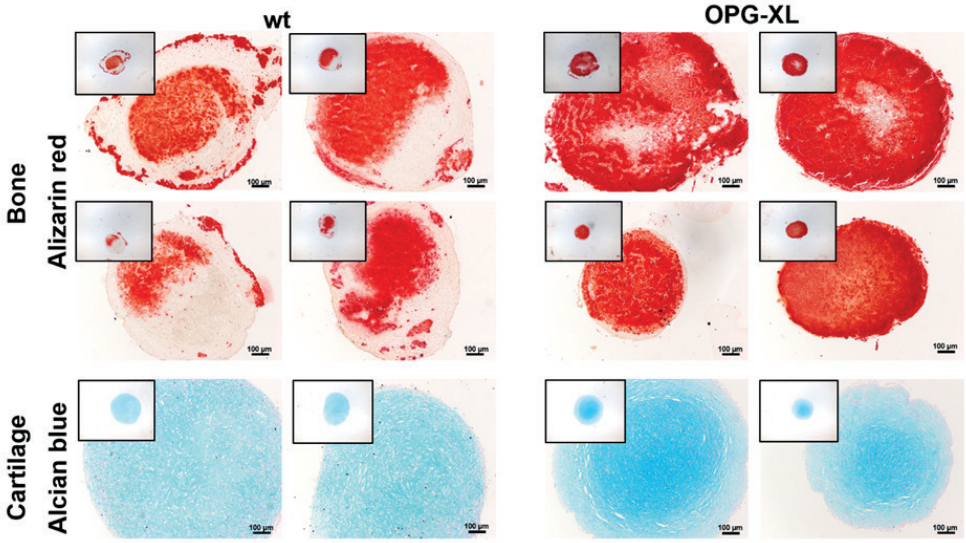

Supplementary Figure S2. Alcian Blue and Alizarin red staining of different neo-cartilage and neo-bone organoids. Histology of organoids resulting from different experiments at day 42 of chondrogenesis stained with Alcian Blue (n=2 independent differentiations) and day 14 of osteogenesis (n=4 independent differentiations) stained with Alizarin red (scale bars: 100µm).

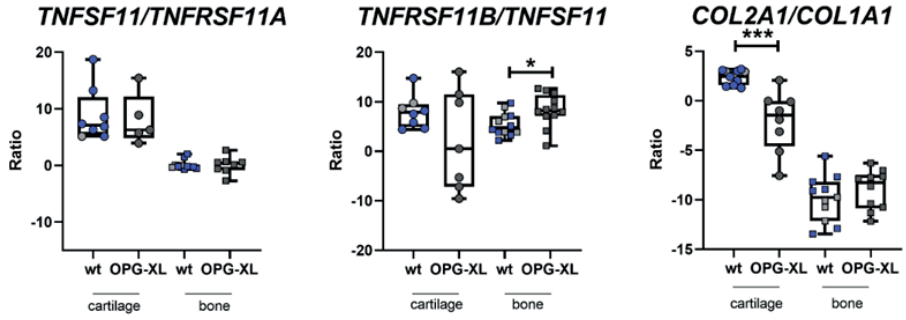

Supplementary Figure S3. Ratios of *TNFSF11/TNFRSF11A*, *TNFRSF11B/TNFSF11* and *COL2A1/COL1A1* in neo-cartilage and neo-bone of the OPG-XL mutation and CRISPR/Cas9-corrected samples. Results shown are at day 42 of chondrogenesis and day 14 of osteogenesis (neo-cartilage: n=9-12 for CRISPR-corrected control and n=5-7 for OPG-XL samples; neo-bone: n=7-14 for CRISPR-corrected control and n=10-16 for OPG-XL samples.; *P-value<0.05; **P-value<10^{-4}; ***P-value<10^{-6}).

Supplementary tables:

Supplementary Table S1. Characteristics of FOA participants.

	OPG-XL non-carriers	OPG-XL carriers
Sex (%)		
Male	66.7	42.9
Female	33.3	57.1
Age (years)		
Minimum	23.1	32.5
Maximum	60.5	61.6
Average	41.7 ± 14.3	51.7 ± 12.3
BMI (Kg/m^2)		
Minimum	22.3	24.9
Maximum	29.1	30.1
Average	24.8 ± 3	27.0 ± 1.9

OPG-XL: high impact readthrough mutation in *TNFRSF11B* at CCAL1 locus.

Supplementary Table S2. Skeletal characteristics of participants determined with DEXA scans at different regions of the skeleton.

A

DEXA	OPG-XL non-carriers	Healthy controls
BMD (g/cm2)		
Skull	2.5 ± 0.3	2.5 ± 0.3
Femoral neck	0.9 ± 0.1	0.9 ± 0.1
Narrow neck	1.1 ± 0.2	1.1 ± 0.1
Lumbar spine	1.1 ± 0.2	-
Total body	1.1 ± 0.2	1.2 ± 0.1
Total hips	1.0 ± 0.1	1.0 ± 0.1
Narrow neck width (cm)	3.6 ± 0.4	3.5 ± 0.4

Results presented are the average of OPG-XL non-carriers (N=7) versus non-related healthy controls (N=253).

B

DEXA	OPG-XL non-carriers	OPG-XL carriers	P value [a]
BMD (g/cm²)			
Skull	2.5 ± 0.3	2.3 ± 0.5	$4.3x10^{-1}$
Femoral neck	0.9 ± 0.1	0.7 ± 0.1	**$1.8x10^{-2}$**
Narrow neck	1.1 ± 0.2	0.8 ± 0.1	**$4.5x10^{-3}$**
Lumbar spine	1.1 ± 0.2	1.1 ± 0.2	$8.8x10^{-1}$
Total body	1.1 ± 0.2	1.2 ± 0.2	$1.8x10^{-1}$
Total hips	1.0 ± 0.1	0.8 ± 0.1	**$7.2x10^{-3}$**
Narrow neck width (cm)	3.6 ± 0.4	3.9 ± 0.2	**$4.1x10^{-4}$**
T-score			
Hips	-0.1 ± 1.4	-1.4 ± 0.6	**$1.2x10^{-2}$**
Lumbar spine	-0.1 ± 1.5	0.2 ± 1.8	$8.8x10^{-1}$
MOAKS			
BML and Cysts (#)	0.3 ± 0.5	18.6 ± 14.1	**$2.4x10^{-5}$**

Results presented are the average of FOA members (7 carriers versus 6 non-carriers of the OPG-XL mutation; # number).

[a]P-value was determined by performing a generalized estimation equation (GEE), with BMD, Narrow neck, T-score, and BML and cysts as dependent variable, and age, sex and BMI as covariate.

OPG-XL: high impact readthrough OPG mutation at CCAL1 locus.

Supplementary Table S3. MOAKS grading of knee joints.

MOAKS	Grades			
Osteophytes (Size)	**0**	**1**	**2**	**3**
OPG-XL non-carrier (%)	95.8 ± 5.3	4.2 ± 5.3	0	0
OPG-XL carrier (%)	30.0 ± 23.3	31.7 ± 13.4	21.7 ± 9.0	16.7 ± 17.7
P value [a]	**$6.8x10^{-4}$**	**$2.3x10^{-4}$**	**$3.4x10^{-4}$**	**$1.7x10^{-3}$**
BML & Cyst (Size)	**0**	**1**	**2**	**3**
OPG-XL non-carrier (%)	98.9 ± 1.7	1.1 ± 1.7	0	0
OPG-XL carrier (%)	57.3 ± 19.6	30.0 ± 7.1	5.3 ± 6.1	7.3 ± 8.3
P value [a]	**$1.7x10^{-10}$**	**$1.0x10^{-30}$**	**$2.0x10^{-2}$**	**$2.4x10^{-2}$**
BML & Cyst (%)	**0**	**1**	**2**	**3**
OPG-XL non-carrier (%)	99.4 ± 1.4	0	0	0.6 ± 1.4
OPG-XL carrier (%)	63.3 ± 17.0	4.7 ± 6.5	4.7 ± 7.3	26.0 ± 7.6
P value [a]	**$2.0x10^{-9}$**	$1.0x10^{-1}$	**$7.3x10^{-2}$**	**$0.0x10^{-30}$**
Cartilage (%)	**0**	**1**	**2**	**3**
OPG-XL non-carrier (%)	91.8 ± 8.1	5.8 ± 5.8	3.0 ± 3.6	0.9 ± 1.5
OPG-XL carrier (%)	56.4 ± 19.3	7.6 ± 4.3	4.4 ± 2.1	33.1 ± 17.3
P value [a]	**$3.7x10^{-4}$**	$7.8x10^{-1}$	$3.6x10^{-1}$	**$4.5x10^{-10}$**

Results presented are the average of FOA members (5 carriers versus 6 non-carriers of the OPG-XL mutation; 2 carriers were excluded due to knee prosthetics).
[a]P-value was determined by performing a generalized estimation equation (GEE), with osteophyte (size), BML and cysts size and percentage, and cartilage percentage as dependent variable, and age, sex and BMI as covariate.
OPG-XL: high impact readthrough OPG mutation at CCAL1 locus.

Supplementary Table S4. Osteoclastogenesis assay of OPG-XL family members against age- and sex-matched controls.

Pair	Participant	Sex	Age
1	Control	Male	49
	OPG-XL	Male	39
2	Control	Female	53
	OPG-XL	Female	62
3	Control	Female	60
	OPG-XL	Female	60
4	Control	Male	65
	OPG-XL	Male	48
5	Control	Male	54
	OPG-XL	Male	59
6	Control	Female	57
	OPG-XL	Female	61

OPG-XL: individual with familial early-onset osteoarthritis, carrier of high impact readthrough mutation in *TNFRSF11B* at CCAL1 locus.

Supplementary Table S5. Matrix, mineralization, osteoclastogenesis and housekeeping primer sequences.

Matrix Genes	**Fwd**	**Rvs**
ADAMTS5	5′-CGTGTACTTGGGCGATGACA-3′	5′-CTGTTGTTGCACACCCCTCT-3′
ACAN1	5′AGAGACTCACACAGTCGAAACAGC-3′	5′-CTATGTTACAGTGCTCGCCAGTG-3′
COL10A1	5′-GGCAACAGCATTATGACCCA-3′	5′-TGAGATCGATGATGGCACTCC-3′
COL1A1	5′-GTGCTAAAGGTGCCAATGGT-3′	5′-ACCAGGTTCACCGCTGTTAC -3′
COL2A1	5′-CTACCCCAATCCAGCAAACGT-3′	5′-AGGTGATGTTCTGGGAGCCTT-3′
COMP	5′-ACAATGACGGAGTCCCTGAC-3′	5′-TCTGCATCAAAGTCGTCCTG-3′
MMP13	5′-TTGAGCTGGACTCATTGTCG-3′	5′-GGAGCCTCTCAGTCATGGAG-3′
SOX9	5′-CCCCAACAGATCGCCTACAG-3′	5′-CTGGAGTTCTGGTGGTCGGT-3′
SMAD3	5′-GCCCCTTTCAGGTAACCGTC-3′	5′-GAAGCGGCTGATGCTCCTTA-3′
MMP3	5′-GAGGCATCCACACCCTAGGTT-3′	5′-TCAGAAATGGCTGCATCGATT-3′
Mineralization genes	**Fwd**	**Rvs**
ALPL	5′-CAAAGGCTTCTTCTTGCTGGTG-3′	5′-CCTGCTTGGCTTTTCCTTCA-3′
ASPN	5′-ACACGTTTTGGAAATGAGTGC-3′	5′-GAACACCGTCACCCCTTCAA-3′
MGP	5′-CGCCCCCAGATTGATAAGTA-3′	5′-TCTCCTTTGACCCTCACTGC-3′
POSTN	5′-TACACTTTGCTGGCACCTGT-3′	5′-TTTAAGGAGGCGCTGATCCA-3′
RUNX2	5′-CAATTTCCTCCTTGCCCCTCA-3′	5′-TCGGATCTACGGGAATACGCA-3′
SPP1	5′-GCCAGTTGCAGCCTTCTCA-3′	5′-AAAAGCAAATCACTGCAATTCTCA-3′
TNFRSF11A	5′-GAAGCTCAGCCTTTTGCTCA-3′	5′-GGGAACCAGATGGGATGTCG-3′
TNFRSF11B	5′-TTGATGGAAAGCTTACCGGGA-3′	5′-TCTGGTCACTGGGTTTGCATG-3′
TNFSF11	5′-CAACAAGGACACAGTGTGCAA-3′	5′-AGGTACAGTTGGTCCAGGGT-3′
DIO2	5′-TTCCAGTGTGGTGCATGTCTC-3′	5′-AGTCAAGAAGGTGGCATGTGG-3′
IL11	5′-CTCTACAGCTCCCAGGTGTGC-3′	5′-AGGTAGGACAGTAGGTCCGCT-3′
SOST1	5′-GAGCTGGAGAACAACAAGACCA-3′	5′-AGCTGTACTCGGACACGTCTTTG-3′
Osteoclastogenesis genes	**Fwd**	**Rvs**
NFATc1	5′-AGCAGAGCACGGACAGCTATC-3′	5′-GGTCAGTTTTCGCTTCCATCTC-3′
DC-STAMP	5′-ATTTTCTCAGTGAGCAAGCAGTTTC-3′	5′-AGAATCATGGATAATATCTTGAGTTCCTT-3′
TRAcP	5′-CACAATCTGCAGTACCTGCAAGAT-3′	5′-CCCATAGTGGAAGCGCAGATA-3′
Cathepsin K	5′-CCATATGTGGGACAGGAAGAGAGTT-3′	5′-TGCATCAATGGCCACAGAGA-3′
Housekeeping genes	**Fwd**	**Rvs**
GAPDH	5′-TGCCATGTAGACCCCTTGAAG-3′	5′-ATGGTACATGACAAGGTGCGG-3′
ARP	5′-CACCATTGAAATCCTGAGTGATGT-3′	5′-TGACCAGCCGAAAGGAGAAG-3′

Supplementary Table S6. Gene expression analyses of primary chondrocytes of an OPG-XL carrier compared against healthy controls.

Extracellular matrix genes				
Genes	**FD**	**Beta**	**SE**	**P value [a]**
COL1A1	**13.8**	**3.8**	**0.3**	**$1.0x10^{-30}$**
COL2A1	-1.8	-0.8	0.6	$1.3x10^{-1}$
COL10A1	**6.9**	**2.8**	**0.3**	**$8.6x10^{-16}$**
ACAN	1.2	0.3	0.4	$4.7x10^{-1}$
SOX9	2.4	1.2	0.7	$7.8x10^{-2}$
ADAMTS5	-1.5	-0.6	1.0	$5.4x10^{-1}$
MMP13	**5.6**	**-2.5**	**0.6**	**$1.0x10^{-5}$**

Results presented are the average of one carrier of the OPG-XL mutation (8 replicates) versus five independent OA patients that underwent joint replacement surgery following three weeks of chondrogenesis.

[a]P-value was determined by performing a generalized estimation equation (GEE) of -ΔCT values, with every independent gene as a dependent variable, and mutation condition as covariate.

Supplementary Table S7. Number of osteoclasts (>3 nuclei) formed in osteoclastogenesis.

Cells/cm² at 14 days	Patient 1		Patient 2		Patient 3		Patient 4		Patient 5		Patient 6		Average	
Nuclei/cell	**Control**	**OPG-XL**	**Control**	**OPG-XL**	**Control**	**OPG-XL**	**Control**	**OPG-XL**	**Control**	**OPG-XL**	**Control**	**OPG-XL**	**Control**	**OPG-XL**
3-5	353.2	123.4	110.9	46.9	134.4	57.8	337.5	62.5	339	125	210.9	100	263	86
6-10	70.3	4.7	4.7	1.6	21.9	0	31.3	3.1	29.7	6.3	20.3	7.8	30	4
11-20	4.7	0	0	0	4.7	0	1.6	0	3.1	0	4.7	0	3	0
> 20	0	0	0	0	0	0	0	0	0	0	0	0	0	0
Total	428.1	128.1	115.6	48.4	160.9	57.8	370.3	65.6	371.9	131.3	235.9	107.8	295	90
Cells/cm² at 21 days	**Patient 1**		**Patient 2**		**Patient 3**		**Patient 4**		**Patient 5**		**Patient 6**		**Average**	
Nuclei/cell	**Control**	**OPG-XL**	**Control**	**OPG-XL**	**Control**	**OPG-XL**	**Control**	**OPG-XL**	**Control**	**OPG-XL**	**Control**	**OPG-XL**	**Control**	**OPG-XL**
3-5	656.3	484.4	551.6	189.1	545.3	253.1	689.1	365.6	854.7	165.6	578.1	284.4	644	290
6-10	134.4	171.9	120.3	198.4	81.3	43.8	59.4	109.4	92.2	109.4	114.1	53.15	94	114
11-20	6.3	71.9	25	65.6	4.7	0	4.7	37.5	23.4	73.4	14.1	67.2	13	53
> 20	4.7	15.6	9.4	31.3	7.8	1.6	4.7	12.5	3.1	23.4	4.7	12.5	6	16
Total	801.6	743.8	706.3	484.4	639.1	298.4	757.8	525	973.4	371.9	710.9	417.2	758	473

Results are presented for each participant (FOA members expressing OPG-XL and age- and sex-matched controls) stratified for number of nuclei per osteoclast and counted in triplicate at day 14 and at day 21.
OPG-XL: high impact readthrough mutation in *TNFRSF11B* at CCAL1 locus.